TO BE PUBLISHED: FERRITIC STEELS IN NUCLEAR TECHNOLOGIES, ed. by J. W. Davis and D. J. Michel (AIME, Warrendale, PA). Proc. of the Topical Conf. on Ferritic Alloys for Use in Nuclear Energy Technologies held in Snowbird, Utah, June 19-23, 1983.

SWELLING BEHAVIOR OF A SIMPLE FERRITIC ALLOY

L. L. Horton and J. Bentley

Metals and Ceramics Division
Oak Ridge National Laboratory
Oak Ridge, Tennessee 37831

The swelling behavior which results from simulated fusion environment irradiation of Fe–10% Cr has been characterized with transmission electron microscopy. Specimens were bombarded at 850 K with: a "triple-beam" of He^+, D_2^+, and 4 MeV Fe^{++} ions to 0.3, 1, 3, 10, 30, and 100 dpa (displacement per atom); a "dual-beam" of He^+ and 4 MeV Fe^{++} ions to 30 and 100 dpa; and a "single-beam" of 4 MeV Fe^{++} ions to 30 dpa. The helium and hydrogen injection rates were ~10 appm He/dpa and ~40 appm D/dpa. Cavities were observed for damage levels of 3 dpa and greater. The swelling was <0.1% for damage levels <30 dpa, but at 100 dpa, there was an increase in the swelling to 2.5% for the "triple-beam" irradiation and 1.2% for the "dual-beam" irradiation. The swelling rates between 30 and 100 dpa correlate well with calculated values assuming a steady-state swelling-rate regime has been reached. Calculations show the rapid cavity growth associated with this swelling increase cannot be attributed to equilibrium bubble growth. For all of the bombardments, the cavities with a diameter greater than 10 nm had a truncated octahedral morphology with {111} facets and {100} truncations. Measurements indicate that the surface energy relationship was $\gamma_{111}=0.8\ \gamma_{100}$ for these cavities. At 30 dpa, the cavities in the specimen irradiated with the "single-beam" technique were larger and had a lower concentration than the specimens irradiated with dual- and triple-beam techniques. Comparison of the specimens irradiated with the dual- and triple-ion beams suggests that deuterium has an effect on the damage microstructures in Fe–10% Cr.

1. Introduction

Potential uses of ferritic steels currently include fusion reactor first wall and blanket structural materials. It is difficult to evaluate materials for these applications as no prototype fusion reactors exist. In the fusion environment, the first wall and blanket structure will be bombarded by a large fast-neutron flux, with ~20% of the neutrons having energies ranging from 10 to 14.1 MeV. The neutrons will cause atomic displacements and the formation of transmutation products. When considering radiation damage, helium and hydrogen are the most important of these transmutation products. For evaluation of microstructural damage, ion irradiation procedures involving simultaneous bombardment of specimens with energetic gas and heavy ions are often used. The heavy ions create atomic displacements while the gas ions simulate the effects of transmutation products. Commonly, "dual-beam" irradiations with heavy ions and helium ions are employed. In the "triple-beam" procedure developed at Oak Ridge National Laboratory (ORNL), a deuterium component is added to the helium beam (1–3). The deuterium ions simulate transmutation produced hydrogen.

In the current investigation, both the dual- and triple-beam techniques are employed to study cavity formation in the binary alloy Fe–10% Cr. This alloy was selected because several of the ferritic stainless steels being considered for fusion applications contain ~10% chromium. In addition, transmission electron microscope (TEM) studies of the commercial steels are difficult due to their ferromagnetic-nature and their usually complex pre-irradiation microstructures. The simpler microstructure found in the binary alloy allows more complete characterization of the damage structures. In this paper, the swelling behavior observed for several damage levels is reported.

2. Experimental Procedure

The Fe–10% Cr alloy was fabricated at ORNL from MARZ grade iron (99.99+%) and IOCHROME chromium (99.96+%) obtained from Materials Research Corporation. A full description of the alloy preparation procedure is given elsewhere (4). Rods (3-mm-diam) were annealed in flowing dry hydrogen for 24 h at 1400 K, furnace cooled to 1000 K, held at this temperature for 2 h, and then furnace cooled. Impurity concentrations for the alloy after annealing are shown in Table I. The grain size was ~200 μm. Specimens of ~0.5 mm thickness were sliced from the rods and prepared for ion bombardment using standard techniques (4). TEM examinations indicated that the dislocation density was $<10^{12}$ m^{-2}.

Ion bombardments were performed in the dual Van de Graaff accelerator facility at ORNL (1–3). For the dual-beam procedure, He^+ and 4 MeV Fe^{++} ions were employed. For triple-beam irradiations, D_2^+ ions were also used. The energy of the He^+ or He^+/D_2^+ beam was ramped sinusoidally at 2.5×10^{-2} Hz between 0.2 and 0.4 MeV. This technique distributes the gas ions throughout the damage region created by the heavy ions. A discussion of the damage profiles

Table I. Impurity concentrations in Fe–10% Cr specimen materials (wt ppm)

Element	Concentration	Element	Concentration
C	34	K	7
H	2	Mg	<3
N	4	Mn	10
O	6	Mo	<2
Ag	2	Na	4
As	20	Nb	2
B	2	Ni	20
Ba	4	P	10
Br	5	S	20
Cl	40	Sb	2
Ca	4	Sn	70
Co	4	Ta	<3
Cu	30	V	1
Ga	50	W	<10
Ge	20	Zn	10

and the implanted helium and deuterium profiles for these irradiation conditions has been presented elsewhere. The specimens were irradiated at ~7 × 10^{-3} dpa s^{-1}. The desired gas concentration to displacements ratios were 10 appm He/dpa and 40 appm D/dpa, the ratios expected for a ferritic steel first wall (6,7). Actual values of these ratios for each specimen examined are listed in Table II. The irradiation temperature (T_I) was ~850 K (~575°C) which in a previous study had been determined to be the temperature at which the peak swelling occurred (4,8). Damage levels of 0.3, 1, 3, 10, 30, and 100 dpa were attained in the triple-beam irradiations. Dual-beam experiments were performed for damage levels of 30 and 100 dpa. An additional experiment was also conducted with a single ion beam (4 MeV Fe^{++} only) to 30 dpa. Actual irradiation parameters for the specimens examined are given in Table II. Irradiation temperatures, T_I, were measured with an infrared pyrometer. The displacements per atom (dpa) shown in Table II are calculated from the heavy ion flux measured for each specimen periodically during the experiment.

In these irradiations, as in most ion irradiations, the damage region is within a few micrometers of the irradiated surface. In specimen preparation for TEM examination, the first step was the controlled removal or "sectioning" of the damaged region to a depth of 0.85–0.9 μm, followed by backthinning. The sectioning depth was selected based on the damage-depth profile for iron irradiated at 850 K using the triple-beam technique (4,5). The specimens were sectioned in a vertical jet apparatus with an 80% ethanol–20% perchloric acid solution cooled to ~225 K. Backthinning was performed at ~285 K with a Tenupol electropolishing apparatus and an electrolyte of 900 ml acetic acid, 100 ml methanol, and 100 ml perchloric acid. The specimens were examined at 120 kV in a JEM 120C TEM equipped with a special objective lens pole-piece for the observation of magnetic materials. Several of the specimens were also examined in a JEM 120CX TEM or a Hitachi 1 MV high voltage electron microscope (HVEM).

Table II. Irradiation parameters and quantitative experimental data*

T_I (K)	Nominal dpa	dpa	He (appm/dpa)	D (appm/dpa)	Dislocation Density (m/m^3)	Cavity Parameters: Conc (m^{-3})	Cavity Parameters: Vol av diam (nm)	Cavity Parameters: Swelling (%)
848	0.3	0.3	9	29	3.7×10^{13}	**		
848	1.0	1.0	8	26	3.9×10^{13}	**		
853	3	3	8	28	6.8×10^{13}	3.5×10^{19}	9	0.001
849	10	10	10	20	1.1×10^{14}	2.6×10^{19}	23	0.02
855	10	10	12	39	5.7×10^{13}	3.2×10^{19}	21	0.02
844	30	26	9	29	3.2×10^{13}	$\{2.4 \times 10^{19}$ $1.6 \times 10^{20}\}$	8 22	0.09
867	100	101	9	29	4.8×10^{13}	$\{2.0 \times 10^{19}$ $7.9 \times 10^{19}\}$	40 84	2.5
847	30	26	15	—	1.4×10^{13}	5.7×10^{19}	21	0.03
858	100	108	7	—	9.7×10^{12}	$\{\sim 4.0 \times 10^{22}$ $2.5 \times 10^{20}\}$	2.5 44	1.2
841	30	35	—	—	2.1×10^{13}	7.0×10^{18}	37	0.02

*Brackets indicate a bimodal distribution.

**None observed.

3. Results

Triple-Beam Irradiations

Cavities were observed in specimens irradiated to 3 dpa and above. Typical cavity microstructures for each fluence are shown in Figure 1. The cavity distribution was reasonably homogeneous in all specimens. Zones with no cavities were found near the grain boundaries in the specimens irradiated to 10–100 dpa (no grain boundaries crossed the electron transparent regions of the 3 dpa specimens). The denuded zones are extended to about 500 nm from the grain boundaries in the 30 and 100 dpa specimens (Figure 2). No cavities were observed on the grain boundaries. Cavities were often observed in association with dislocations. Lines of cavities were found as well (Figure 3), another possible indication of cavity growth on dislocations.

For damage levels >10 dpa, the observed cavities had a crystallographic shape. Figure 3 shows micrographs of the cavities in a specimen irradiated to 30 dpa taken near the <100> and <110> poles with $\underline{g}$ = <330>. Analyses of the cavity shapes shown in these micrographs indicated that the cavities had a truncated octahedral shape. The cavity facets are on {111} with truncations on {100}. Comparisons of the micrographs taken near the <100> and <110> poles with computed images of truncated octahedral cavities ({111} facets, {100} truncations) for these orientations (9) supported this conclusion.

The data for the measured dislocation density, cavity concentration (N_c), volume-averaged cavity diameter (d_c), and calculated cavity volume fraction (swelling) are given in Table II. In addition, the cavity data are depicted in Figure 4. The cavity diameters were measured assuming a circular projection with approximately the same area as the crystallographic projection. For 30 and 100 dpa, as indicated in Table II, the measured cavity diameters had a bimodal distribution. In a histogram of the measured cavity diameters for the 30 dpa specimens, about 20% of the cavities were found in a peak centered at ~7 nm while the remaining 80% were in a peak centered at ~20 nm. The volume-averaged cavity diameters for these peaks were 8 and 22 nm. At 100 dpa, the two peaks were less distinct. The

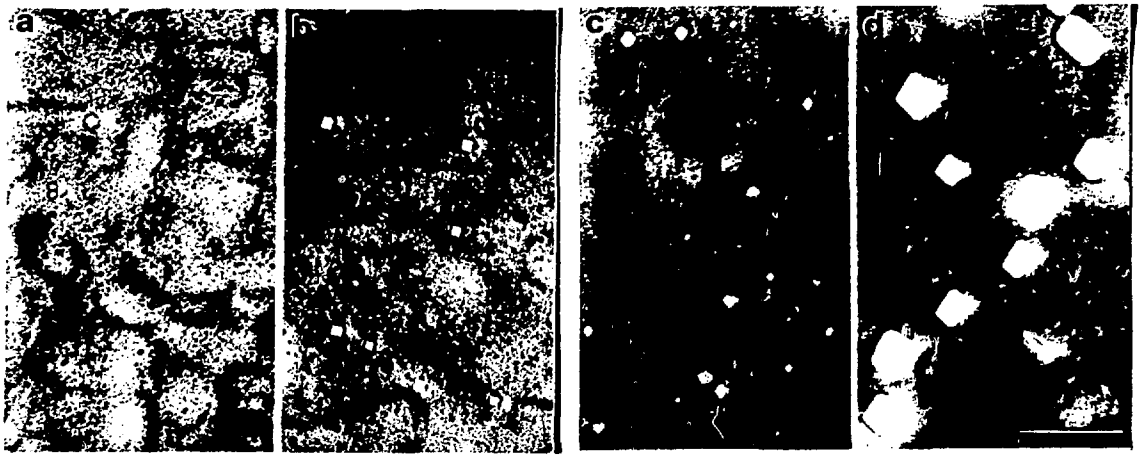

Figure 1 - Cavity microstructures found in triple-beam ion-irradiated Fe–10% Cr. T_I~850 K. Scale marker is 200 nm. (a) 3 dpa, (b) 10 dpa, (c) 30 dpa, and (d) 100 dpa.

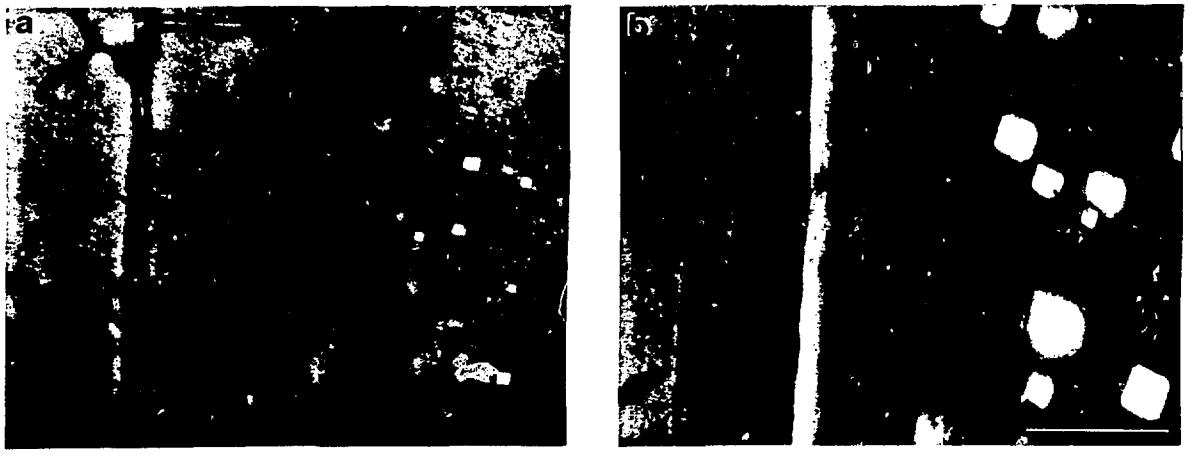

Figure 2 - Zones denuded of cavities found near grain boundaries in triple-beam ion-irradiated Fe–10% Cr. Scale marker is 250 nm. (a) 30 dpa and (b) 100 dpa.

lower peak (~20% of the cavities) had a volume-averaged diameter of 40 nm and the upper peak (~80% of the cavities) had a volume-averaged diameter of 84 nm. In Figure 4, the values at 30 and 100 dpa for the volume-average cavity diameter and the cavity concentration are the values calculated for the entire distribution. Between 30 and 100 dpa, the swelling increased from <0.1% to 2.5%. The possibility of an additional population of very small cavities was considered likely, especially at the higher damage levels. If present, however, these cavities are too small (<2 nm diam) to be visible with TEM.

According to Wulff's theorem, the ratio of the surface energy, γ_{hkl}, to the perpendicular distance, d_{hkl}, between diametrically opposite (hkl) planes which serve as faces of an equilibrium bubble is a constant (10,11). This relationship has been used to measure the ratio of the surface energies of different low index planes for cavities in copper, aluminum, and molybdenum (12). The relationship $\gamma_{111}/d_{111} = \gamma_{100}/d_{100}$ was used to determine the surface energy ratio for the cavities found in the 30 dpa specimen. Both d_{111} and d_{100} were measured for a number of cavities from the cavity projection for a <110> beam direction. Additional measurements of d_{100} were made for each cavity from a projection for a <100> beam direction. The average value for the $\gamma_{111}/\gamma_{100}$ ratios calculated from these measurements was 0.77 with a standard deviation of 0.06.

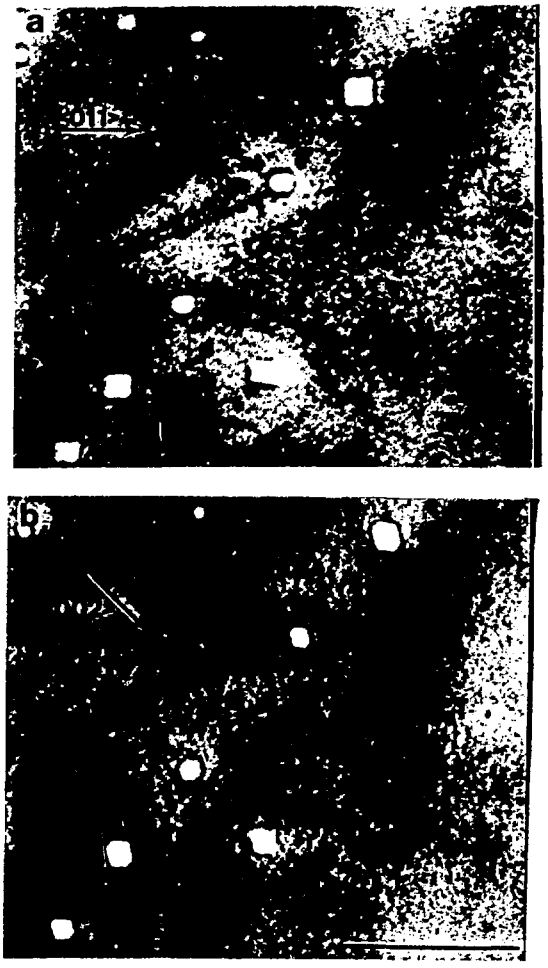

Figure 3 - Crystallographic cavity shape observed in triple-beam ion-irradiated (30 dpa, T_I~850 K) Fe–10% Cr for beam direction near (a) <100> and (b) <110>. Scale marker is 200 nm.

Dual Beam Irradiations

The cavity microstructures observed in the specimens irradiated using the dual-beam technique are shown in Figure 5. At 30 dpa, large (~21 nm av diam) crystallographic cavities were observed. Some of the contrast effects in the micrographs also suggested a background population of not clearly resolvable cavities. At 100 dpa, the cavity distribution was definitely bimodal. In addition to the large (44 nm av diam) crystallographic cavities, there was a high (~4 × 10^{22} m^{-3}) concentration of small, 2.5 nm av diam, cavities observed in the thin areas of the foil (Figure 5c). These small cavities did not have an observable crystallographic shape. The quantitative cavity parameters are shown in Table II. These data are plotted with the triple-beam data for 30 and 100 dpa in Figure 6. For the 30 and 100 dpa triple-beam specimens, the cavities in the two parts of the bimodal distribution are within the same general size class, i.e., have average diameter within a factor of three. Therefore, in Figure 6, the values for the entire distribution are used for these data points. For the 100 dpa dual-beam specimen, however, the cavities in the two parts of the bimodal have more than an order of magnitude difference in the average diameters. In Figure 6, the values for each part of the bimodal distribution are shown for this specimen.

The cavities were often observed in association with dislocations. At 100 dpa, as shown in Figure 7, some of the dislocations appeared to be pinned along their length, possibly by small cavities. Cavities with ~4 nm av diam were found at

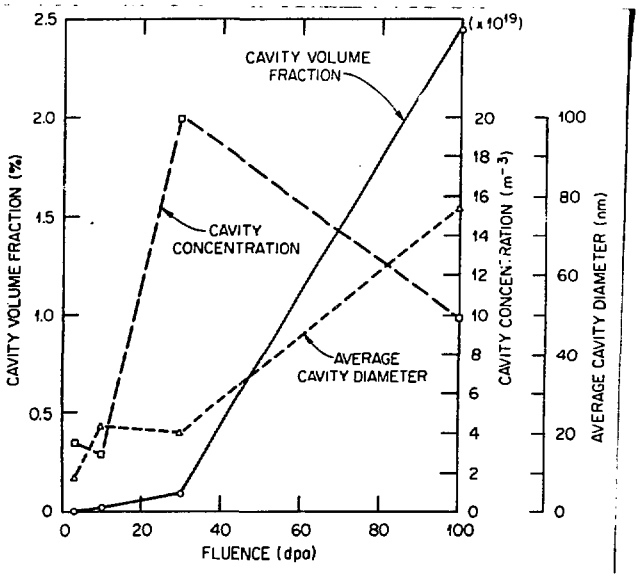

Figure 4 - Quantitative cavity parameters measured for triple-beam ion-irradiated Fe–10% Cr. T_I~850 K.

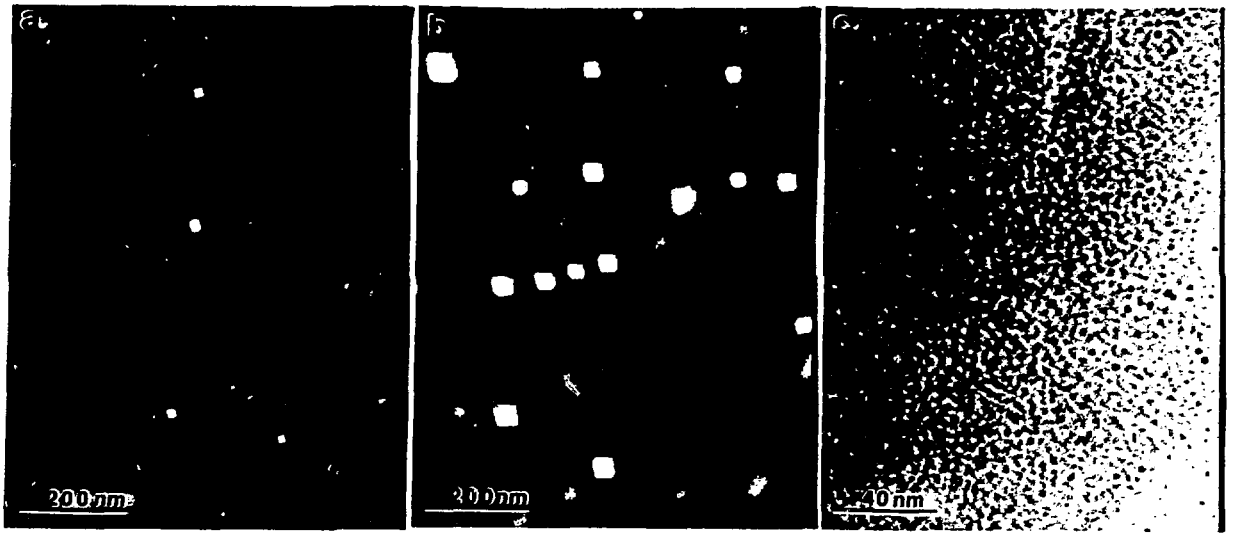

Figure 5 - Cavity microstructures found in dual-beam ion-irradiated Fe–10% Cr. T_I~850 K. (a) 30 dpa, (b) 100 dpa, and (c) 100 dpa, high magnification micrograph showing the 2.5 nm-av-diam cavities over focused image.

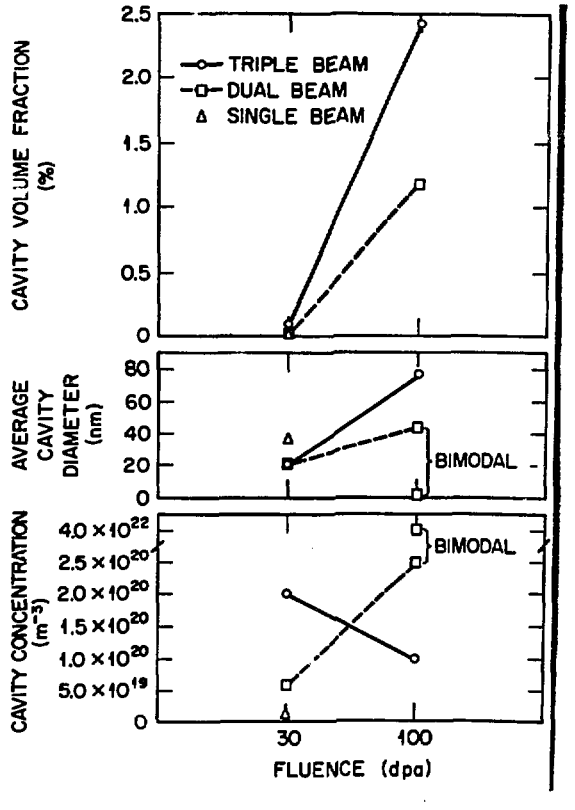

Figure 6 - Comparison of the cavity parameters for single-, dual-, and triple-beam irradiations. T_I~850 K.

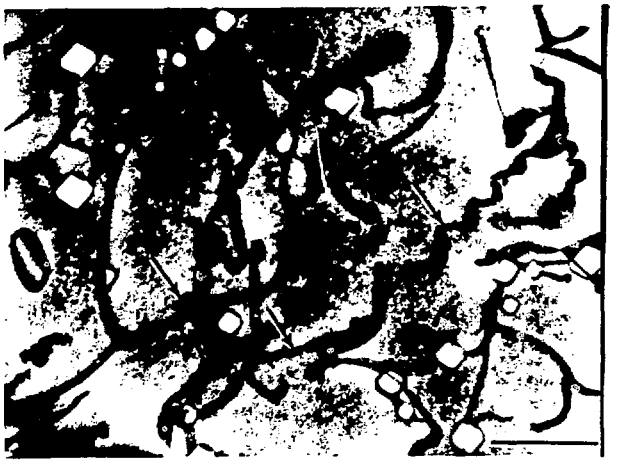

Figure 7 - Dislocations observed in the 100 dpa specimen (dual-beam irradiation). Note the cavities along the dislocations. The bowed appearance of the dislocations marked by arrows suggests pinning by small cavities. Scale marker is 200 nm.

grain boundaries in the 100 dpa specimen (Figure 8). The alignment of many of these cavities (Figure 8a) suggests that they are associated with grain boundary dislocations or ledges. Next to the boundary shown in Figure 8b, there appears to be a narrow, <50 nm wide zone with no cavities. From 50 to 200 nm from the grain boundaries, the concentration of the small, 2.5 nm av diam, cavities increased to the concentration found further from the boundary (Figure 8b). In contrast, the closest of the larger crystallographic cavities were about 500 nm from the boundary. This distance is comparable to that observed for the denuded zones in the 30 and 100 dpa triple-beam specimens.

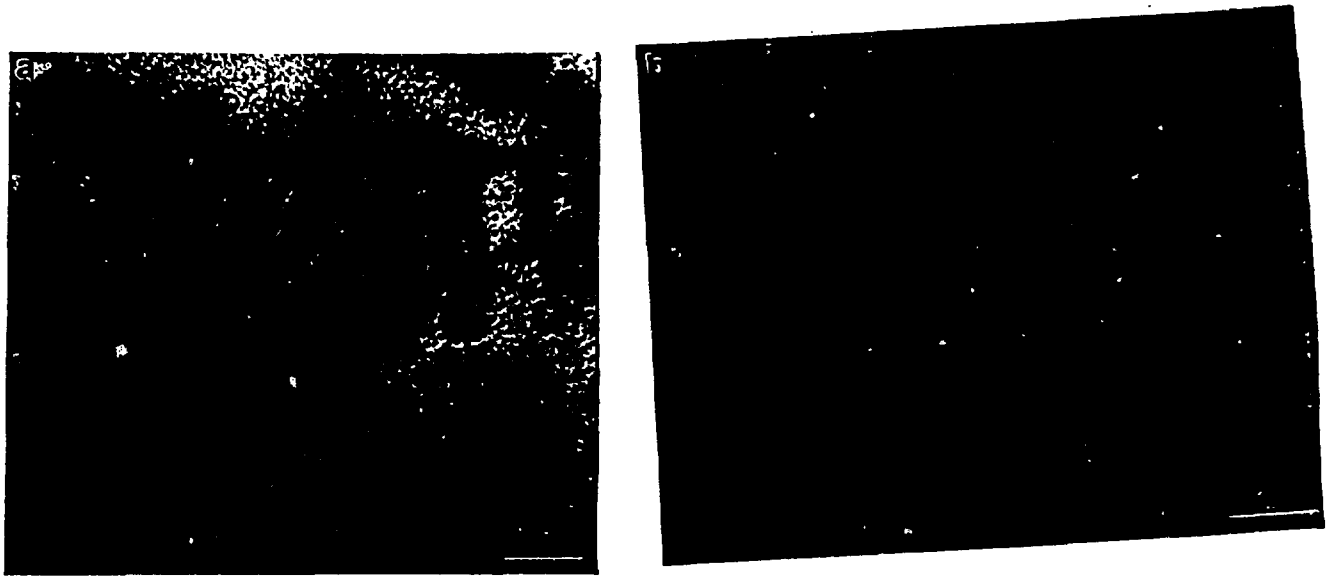

Figure 8 - Grain boundaries observed in dual-beam ion-irradiated Fe–10% Cr, 100 dpa, over focused images. (a) Aligned cavities found on the grain boundaries. (b) Note the decrease in cavity concentration ~200 nm from the boundary. Next to the boundary is a narrow zone (~50 nm wide) denuded of cavities. Scale markers are 50 nm.

The crystallographically-faceted cavities had the same shape as those in the triple-beam specimens. For the cavities found in the 30 dpa specimen, the surface energy ratio, $\gamma_{111}/\gamma_{100}$, calculated from measurements of d_{111} and d_{100} was 0.78 with a standard deviation of 0.06.

Single Ion Irradiations

The micrograph in Figure 9 shows the cavity microstructure found in Fe–10% Cr irradiated with 4 MeV Fe^{++} ions to ~30 dpa. The measured microstructural parameters are found in Table II. The cavities were larger (37 nm av diam) and had a lower concentration (7×10^{18}) than those in the 30 dpa specimens from the dual and triple beam irradiations. The single beam cavity data are plotted with the data from the other irradiations in Figure 6.

Other features of the cavities were similar to many of those presented earlier. The cavities were associated with dislocations, no cavities were found at or near grain boundaries, the crystallographic shape of the cavities was the same as that found for the triple- and dual-beam irradiations, and the surface energy ratio, $\gamma_{111}/\gamma_{100}$, calculated from the d_{111} and d_{100} measurements was 0.81 ± 0.06.

4. Discussion

Cavity Growth Modes

One notable feature observed in this investigation was the dramatic increase in the swelling between 30 and 100 dpa. For the triple-beam irradiations, the increase in the swelling was primarily due to an increase in the volume-averaged cavity diameter from ~20 nm at 30 dpa to ~75 nm at 100 dpa. As an explanation for this rapid growth, the possibility that all of the cavity growth occurred as equilibrium bubble growth was considered. The number of helium atoms per cavity, n_{eq}, required to stabilize the cavities as equilibrium bubbles was calculated using the high-density equation-of-state developed by Wolfer (13). The values for n_{eq}, assuming a surface energy of $2J/m^2$, obtained for the volume-averaged cavity diameters for each fluence are compiled in Table III. Also found in Table III are the values for the total amount of helium required for all of the observed cavities to be equilibrium bubbles. Assuming that all of the available helium is in the observed cavities, a comparison of the available helium concentration to the amount required for equilibrium bubbles suggests that, in general, the apparent "bubble character" of the cavities decreases with increasing damage level. For example, considering the triple-beam data, at 3 dpa there was about a factor of four more helium

Figure 9 - Cavity microstructures found in Fe–10% Cr irradiated with 4 MeV Fe^{++} ions. T_I~850 K, 30 dpa. Scale marker is 200 nm.

available than is required for all cavities to be equilibrium bubbles. At 100 dpa, only ~50% of the helium required for equilibrium bubbles was available. This suggests that the cavities are not growing as equilibrium bubbles at 100 dpa. If partitioning of mobile helium to the dislocations is considered, the amount of helium available for the cavities is significantly reduced, especially at the lower fluences. In addition, the available helium would also be reduced by the presence of a high concentration of small, helium-containing cavities that were not observed in the TEM examinations. This possibility is supported by the high concentration of 2.5-nm-diam cavities observed for the 100 dpa dual-beam irradiation. Such a population of small cavities was not observed at 30 dpa, suggesting that, at 30 dpa, there could be a population of cavities too small to be seen with TEM.

Many features of the cavity distributions at 30 and 100 dpa (triple beam) suggest that the rapid cavity growth may result from the cavity radius exceeding the critical cavity radius, r^{crit}, or from the number of gas atoms in the cavity exceeding the critical number, n_g^*, required for bias-driven cavity growth (14). Both experimental and theoretical investigations are in progress to determine r^{crit} for Fe-10% Cr.

Clearly, experiments at several fluences between 30 and 100 dpa would be helpful in determining the correct explanation for the rapid cavity growth. An understanding of this mechanism would further the development of ferritic alloys with even greater swelling resistance.

Swelling Rate

Referring to the swelling curves in Figure 6, it could be inferred that the steady-state swelling regime is reached between 30 and 100 dpa. If it is assumed that this regime begins at about 30 dpa, the steady-state swelling rate is ~0.03%/dpa for the triple-beam irradiation and ~0.02%/dpa for the dual beam irradiation. This is much lower than the swelling rate of 0.12%/dpa reported by Johnston et al. (15) for 5 MeV nickel-ion bombardments of 85% Fe-15% Cr specimens which had been preinjected with 25 appm He.

The swelling rate is expected, however, to be sensitive to the balance of the sink strengths of the microstructural components. The maximum values occurs when the cavity sink strength, $2\pi d_c N_c Z^c$, equals the dislocation sink strength, $Z^d L$; where L is the dislocation density and $Z^{c,d}$ are the respective sink capture efficiencies. Recent calculations by Sniegowski and Wolfer (16) have predicted that the maximum steady state swelling rate for ferritic alloys is ~0.14%/dpa for a vacancy relaxation volume of -0.5Ω and an interstitial relaxation volume of 0.9Ω, where Ω is the atomic volume. In this calculation, vacancy reemission from the cavities is ignored. Assuming that $Z^v = Z^d = 1$, at 100 dpa for the dual-beam irradiation, the cavity sink strength is $1.1 \times 10^{14} m^{-2}$ while the dislocation sink strength is $9.7 \times 10^{12} m^{-2}$. Thus, the cavity sink strength is a factor of ~11 greater than the dislocation sink strength. Applying these values to the equations used by Sniegowski and Wolfer yields a steady-state swelling rate of ~0.04%/dpa — within a factor of two of the experimental results. For T_I, ~850 K, vacancy reemission should probably be included in the calculation, which would lower the calculated swelling rate and improve agreement with the measured values. For the triple-beam irradiation, it seems likely that there is a high concentration of small cavities similar to that found in the dual-beam irradiation. If a $4 \times 10^{22} m^{-3}$ concentration of 1-nm-diam cavities is assumed, the calculated swelling rate is ~0.06%/dpa — once again in good agreement with measured value. In these calculations, it has been assumed that the small (<2.5 nm av diam) cavities are growing by bias-driven growth and have the same capture efficiency as the larger cavities. If this is not the case, the cavity sink strength would change, and the calculated swelling rates could be quite different (14).

Table III. Comparison of the available helium with the helium required for equilibrium bubbles for each specimen. Also shown is n_{eq}, the number of helium atoms per cavity required for a cavity with diameter d_c to be an equilibrium bubble*

Irradiation	Nominal dpa	Helium available (atoms m^{-3})	d_c (nm)	n_{eq} (atoms)	N_c (m^{-3})	Total helium required for equilibrium bubbles (atoms m^{-3})
Triple beam	3	2.0×10^{24}	9	1.4×10^4	3.5×10^{19}	4.9×10^{23}
	10	8.5×10^{24}	23	1.3×10^5	2.6×10^{19}	3.4×10^{24}
	10	1.0×10^{25}	21	1.1×10^5	3.2×10^{19}	3.5×10^{24}
	30	2.0×10^{25}	8	1.1×10^4	4.4×10^{19}	4.8×10^{23}
			22	1.2×10^5	1.6×10^{20}	1.9×10^{25}
			40	4.5×10^5	2.0×10^{19}	9.0×10^{24}
	100	7.7×10^{25}	84	2.1×10^6	7.9×10^{19}	1.7×10^{26}
Dual beam	30	3.3×10^{25}	21	1.1×10^5	5.7×10^{19}	6.3×10^{24}
	100	6.4×10^{25}	2.5	6.1×10^2	$\sim 4.0 \times 10^{22}$	2.4×10^{25}
			44	5.5×10^5	2.5×10^{20}	1.4×10^{26}

*The small brackets indicate bimodal distributions.

These swelling rates are much lower than the ~1%/dpa usually found for the steady-state regime in austenitic materials. If a rate of ~0.03%/dpa is sustained at higher fluences, the swelling would reach 6% at about 200 dpa, roughly equivalent to 20 MWyr-m^{-2} (6). Once again, additional experiments at intermediate damage levels between 30 and 100 dpa would help to clarify the location of the steady-state swelling regime and would allow more accurate projections of the long range swelling behavior.

Cavity Shape

For thermal equilibrium, the expected morphology of cavities is that which produces the *minimum* surface energy, γ, for a specific volume. This shape can be derived from a Wulff construction. In bcc materials, the expected surface energy relationship for the low-index planes is $\gamma_{110} < \gamma_{100} < \gamma_{111}$, as has been found, for example, in molybdenum (12). Thus, the expected and commonly observed morphology in bcc materials is a truncated dodecahedron with {110} facets and {100} truncations. It is not considered unusual, however, to observe cubic cavities with {100} sides. These types of cavity morphologies have been reported for irradiated ferritic materials. Kulcinski et al. (17) reported "truncated octahedral" cavities with {110} faces and {110} truncations in neutron-irradiated iron. Ohnuki et al. (18) have reported cubic cavities with {100} faces in C^+ irradiated iron.

The cavity morphology observed in this investigation, a truncated octahedron with {111} facets and {100} truncations, is the morphology usually found in irradiated fcc materials. Previous investigations have reported a similar morphology for neutron-irradiated iron (19) and iron-chromium alloys (20). The formation of truncated octahedral cavities with {111} faces could be due to surface energy variations caused by impurities preferentially segregating to a specific set of planes. Impurities have been shown to affect cavity shape. For example, in fcc copper, bubbles with {100} and {110} facets are reported for "clean" foils while bubbles with {111} and {100} facets develop in regions exposed to oxygen (12). This is consistent with preferential adsorption of oxygen on the {111} and {100} planes in copper. In the current study, measurements of the surface energy ratio, $\gamma_{111}/\gamma_{100}$, from the cavity geometry in the Fe–10% Cr specimens, indicated that $\gamma_{111} \approx 0.80\ \gamma_{100}$. This relationship was not significantly affected by the irradiation procedure. The observation of no {110} facets suggests that γ_{110} is greater than both γ_{111} and γ_{100}. Thus $\gamma_{111} < \gamma_{100} < \gamma_{110}$ – exactly the opposite of the expected surface energy relationship.

The unexpected shape could also be a result of non-equilibrium conditions during cavity growth. Further experiments – e.g., postirradiation annealing – would show if the cavities have a non-equilibrium shape.

Gas Effects

Comparisons of the cavity parameters for the single-, dual- and triple-beam irradiation procedures are found in Figure 6. For 30 dpa, the cavities observed in the specimen bombarded with only Fe^{++} ions are larger and have a lower concentration than the cavities in the specimens bombarded with both gas and Fe^{++} ions. This result is consistent with the helium effects observed for other materials. For example, a higher concentration of smaller cavities has been observed in austenitic stainless steel irradiated with a dual beam of nickel and helium ions as compared to the cavity distribution found in specimens irradiated with only nickel ions (21,22).

Comparison of Fe–10% Cr specimens irradiated with the dual- and triple-beam procedures yields a more complex relationship. For 30 dpa, the average cavity diameters are about the same while the cavity concentration is higher for the triple-beam irradiation than for the dual-beam irradiation. However, at 100 dpa this relationship is reversed – the observed cavity concentration is much higher for the dual-beam irradiated specimen. The distribution found at 100 dpa for the dual-beam procedure was clearly bimodal (i.e., >99% of the cavities were found to have an average diameter of 2.5 nm while <1% of the cavities had an average diameter of 44 nm). It seems probable, as suggested earlier, that a similar concentration of cavities which are too small to be seen with TEM exists in the triple-beam specimens. If only the larger cavities observed at 100 dpa for both bombardments are considered, however, the average cavity diameter is larger and the concentration is lower for the triple-beam irradiations than for the dual-beam irradiations.

In a similar study with an austenitic alloy (similar in composition to type 316 stainless steel), the average cavity diameter was somewhat larger, and the cavity concentration was slightly lower for triple-beam irradiation than for dual-beam irradiation at 10 dpa ($T_I \sim 900$ K). The opposite was reported for 70 dpa – the average diameter was smaller, and the concentration was higher for the triple-beam irradiation than for the dual-beam (21). These relationships varied erratically for other irradiation temperatures (22). Moreover, at 70 dpa for the austenitic alloy, comparing the dual- and triple-beam data shows that, in general, the variation in the average diameter and concentration was not significant, i.e., much less than a factor of two for the diameter and less than an order of magnitude for the concentration, regardless of irradiation temperature (22). As discussed earlier, at 100 dpa in the ferritic alloy of this study, the differences in the dual- and triple-beam specimens are more substantial. Further study is required before the differences between the dual- and triple-beam irradiations can be clearly defined and understood. These preliminary results do suggest, however, that deuterium (hydrogen) may play a more significant role in the swelling evolution in the ferritic alloys than has been reported for austenitic alloys.

5. Conclusions

This investigation of the swelling characteristics for ion-bombarded Fe–10% Cr has shown:

1. There was a dramatic increase in the average cavity diameter between 30 and 100 dpa for dual- and triple-beam irradiation. Calculations have shown that growth as equilibrium bubbles was not responsible. Examination of specimens irradiated to intermediate damage levels would aid in understanding the cavity growth mechanisms.

2. The swelling rate between 30 and 100 dpa was estimated as 0.02%/dpa for dual-beam irradiations and 0.03%/dpa for triple-beam irradiations. Calculated values for the steady state swelling rate for the sink strengths measured at 100 dpa are within a factor of two of these experimental values.

3. The cavities were truncated octahedra with {111} facets and {100} truncations, the morphology commonly observed for fcc materials. Measurements of the cavity geometry yielded a surface energy ratio, $\gamma_{111}/\gamma_{100}$, of ~0.80.

4. Cavities were found on the boundary only in the dual-beam specimen at 100 dpa. For both the dual- and triple-beam bombardments, no large, crystallographic cavities were observed within 500 nm of the grain boundaries. For the dual-beam specimen at 100 dpa, the denuded zone for the small, 2.5 nm av diam, cavities was <50 nm wide.

5. At 30 dpa a smaller concentration of larger cavities was observed for single ion (Fe^{++}) irradiation than for dual- or triple-beam irradiations.

6. Comparisons of specimens irradiated with the dual- and triple-beam procedures suggests that deuterium may have a significant role in the cavity evolution for ferritic materials. Further study is required before this difference can be clearly defined.

Acknowledgements

The authors would like to thank M. B. Lewis, Y. K. Chang, S. W. Cook, H. Harmon, J. T. Houston, K. F. Russell, and W. H. Smith for assistance with various aspects of specimen preparation; L. K. Mansur, N. H. Packan, and J. M. Vitek for technical comments; and J. G. Turner and J. F. Young for manuscript preparation.

Research was sponsored by the Division of Materials Sciences, U.S. Department of Energy under contract W-7405-eng-26 with the Union Carbide Corporation.

References

(1) K. Farrell, M. B. Lewis, and N. H. Packan, "Simultaneous Bombardment with Helium, Hydrogen, and Heavy Ions to Simulate Microstructural Damage from Fission or Fusion Neutrons," Scripta Met., 12 (1978) pp. 1121–1124.

(2) M. B. Lewis, N. H. Packan, G. F. Wells, and R. A. Buhl, "Improved Techniques for Heavy-Ion Simulation of Neutron Radiation Damage," Nucl. Inst. & Methods, 167 (1979) pp. 233–247.

(3) M. B. Lewis, Trans. Nucl. Sci., NS-26 (1979) pp. 1320–1322.

(4) L. L. S. Horton, A Transmission Electron Microscope Study of Fusion Environment Radiation Damage in Iron and Iron-Chromium Alloys, Ph.D. Dissertation, University of Virginia (May 1982); also published as ORNL/TM-8303 (July 1982).

(5) L. L. Horton, J. Bentley, and W. A. Jesser, "The Depth Distribution of Displacement Damage in α-Iron under 'Triple Beam' Ion Irradiations," J. Nucl. Mater., 103&104 (1981) pp. 1343–1348.

(6) E. E. Bloom, "Mechanical Properties of Materials in Fusion Reactor First-Wall and Blanket Systems," J. Nucl. Mater., 85&86 (1979) pp. 795–804.

(7) T. A. Gabriel, B. L. Bishop, and F. W. Wiffen, "Calculated Atom Displacement and Gas Production Rates of Materials Using a Fusion Reactor First Wall Spectrum," Nucl. Technol., 38 (1978) pp. 427–433.

(8) L. L. Horton, J. Bentley, and W. A. Jesser, "The Microstructure of 'Triple Beam' Ion Irradiated Fe and Fe-Cr Alloys," J. Nucl. Mater., 103&104 (1981) pp. 1085–1090.

(9) A. J. E. Foreman, H. S. Von Harrach, and D. K. Saldin, "The TEM Contrast of Faceted Voids," Phil. Mag., 45(4) (1982) pp. 625–645.

(10) G. Wulff, Z. Kristallog., 34 (1901) p. 449.

(11) C. Herring, "The Use of Classical Macroscopic Concepts in Surface-Energy Problems, pp. 5–72 in Structure and Properties of Solid Surfaces, R. Gomer and C. S. Smith, ed.; University of Chicago Press, Chicago, IL, 1953.

(12) R. A. Nelson, D. J. Mazey, and R. S. Barnes, "The Thermal Equilibrium Shape and Size of Holes in Solids," Phil. Mag., 11 (1965) pp. 91–111.

(13) W. G. Wolfer, "High Density Equation of State for Helium and Its Application to Bubbles in Solids," pp. 201–212 in Effects of Radiation on Materials, ASTM-STP-725, D. Kramer, H. R. Brager, and J. S. Perrin, eds.; ASTM, Baltimore, MD, 1981.

(14) L. K. Mansur and W. A. Coghlan, "Mechanisms of Helium Interaction with Radiation Effects in Metals and Alloys," to be published in J. Nucl. Mater.

(15) W. G. Johnston, T. Lauritzen, J. H. Rosolowski, and A. M. Turkalo, "Void Swelling of Ferritic Alloys Bombarded with Nickel Ions," pp. 809–823 in Effects of Radiation on Materials: Eleventh Conference, ASTM-STP-782, H. R. Brager and J. S. Perrin, eds.; ASTM, Baltimore, MD, 1982.

(16) J. J. Sniegowski and W. G. Wolfer, "On the Physical Basis for the Swelling Resistance of Ferritic Steels," this proceedings.

(17) G. L. Kulcinski, B. Mastel, and J. L. Brimhall, "Formation of Voids in Iron During High Temperature Neutron Irradiation," Rad. Effects, 2 (1969) pp. 57–59.

(18) S. Ohnuki, H. Takahashi, and T. Takeyama, "Void Swelling and Segregation of Solute in Iron-Irradiated Ferritic Steels," J. Nucl. Mater., 103&104 (1981) pp. 1121–1125.

(19) L. L. Horton, J. Bentley, and K. Farrell, "A TEM Study of Neutron-Irradiated Iron," J. Nucl. Mater., 108&109 (1982) pp. 222–233.

(20) D. S. Gelles, "Microstructural Examination of Neutron Irradiated Simple Ferritic Alloys," J. Nucl. Mater., 108&109 (1982) pp. 515–536.

(21) N. H. Packan and K. Farrell, "Simulation of First Wall Damage: Effects of the Method of Gas Implantation," J. Nucl. Mater., 85&86 (1979) pp. 677–681.

(22) K. Farrell and N. H. Packan, "A Helium-Induced Shift in the Temperature Dependence of Swelling," J. Nucl. Mater., 85&86 (1979) pp. 683–687.

DISCLAIMER